13TH INTERNATIONAL ERCOFTAC SYMPOSIUM ON ENGINEERING, TURBULENCE, MODELLING AND MEASUREMENTS
GREECE, 15-17 SEPTEMBER, 2021

Investigation of turbulence statistics in two-phase gas-liquid flow

R. Boukharfane[1], S. Benjelloun[1], M. Parsani[2] & N. Chakraborty[3]

[1] MOHAMMED VI POLYTECHNIC UNIVERSITY, MSDA, BENGUERIR, MOROCCO
[2] KING ABDULLAH UNIVERSITY OF SCIENCE AND TECHNOLOGY, ECRC, THUWAL, SAUDI ARABIA
[3] NEWCASTLE UNIVERSITY, SCHOOL OF ENGINEERING, NEWCASTLE, UNITED KINGDOM

Overview

1. Motivation & Purpose
2. Numerical methods & DNS database
3. Numerical results
4. Conclusion & Perspectives

Motivation & Purpose

General introduction

- Two-phase gas–liquid turbulent flows featuring phase changes are encountered in many natural and industrial processes

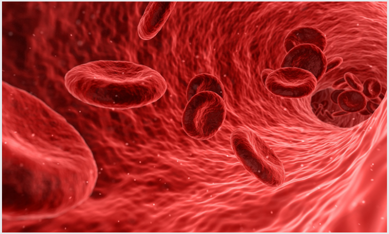

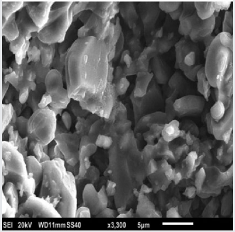

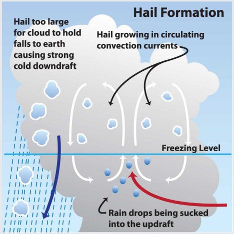

- Effectiveness depends on many parameters
  - Volume and residence time of discrete phase, bubble rise velocity, bubble size or bubble size distribution, and bubble deformability.
- Numerical simulations could be of significant use if adapted models and methods are carefully developed

Motivation

- Study of the velocity gradient tensor (VGT) $\mathcal{A}_{ij} = \partial \mathcal{U}_i / \partial x_j$ in turbulent flows.
- VGT contains all the necessary information
- Its role may be made explicitly by taking the spatial gradient of NS equations

$$\partial \mathcal{A}/\partial t + \mathcal{U} \cdot \nabla \mathcal{A} = -\mathcal{A}^2 - \mathcal{H} + \nu \nabla^2 \mathcal{A}, \text{ where } \mathcal{H}_{ij} = \partial^2 \mathcal{P} / \partial x_i \partial x_j$$

Study of the velocity gradient tensor

Hermitian and skew-Hermitian decomposition approach

$$\mathcal{A} = \mathcal{S}^{\mathcal{A}} + \mathbf{\Omega}^{\mathcal{A}}, \; \boldsymbol{\omega} = \nabla \times \mathcal{U}$$

alignment between the vorticity vector/scalar gradient and the eigenvectors of the strain rate tensor $\mathcal{S}^{\mathcal{A}}$

Eigenvalue-based approach†

$$\lambda_i^3 + P^{\mathcal{A}} \lambda_i^2 + Q^{\mathcal{A}} \lambda_i + R^{\mathcal{A}} = 0$$

$P^{\mathcal{A}} Q^{\mathcal{A}} R^{\mathcal{A}}$ invariants with the identities

$$P^{\mathcal{A}} = \sum_i \lambda_i, \; Q^{\mathcal{A}} = \sum_{i<j} \lambda_i \lambda_j, \; R^{\mathcal{A}} = \prod_i \lambda_i$$

† Chong, M. S., Perry, A. E.
A general classification of three-dimensional flow fields
Physics of Fluids (1990).

➯ Four non-degenerative topologies are possible in the $\left(Q^{\mathcal{A}}, R^{\mathcal{A}}\right)$ phase plane †

- UFC Unstable Focus / Compressing
- UNSS Unstable Node / Saddle / Saddle
- SNSS Stable Node / Saddle / Saddle
- SFS Stable Focus / Stretching

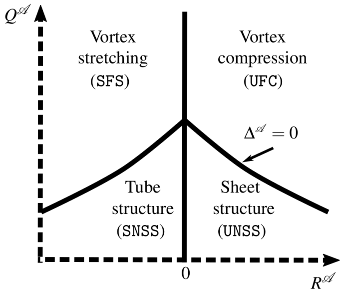

† Ooi, A. and Martin, J.d Soria, J. and Chong, M. S.
A study of the evolution and characteristics of the invariants of the velocity-gradient tensor in isotropic turbulence
Journal of Fluid Mechanics (1999).

Purpose

- Unify eigenvalue-based approach and Hermitian/Skew-Hermitian approaches through a recently proposed Schur decomposition approach[‡]

$$\mathcal{A} = \mathcal{B}^{\mathcal{A}} + \mathcal{C}^{\mathcal{A}}$$

- Use this decomposition to evaluate the influence of the compressibility on some statistical properties of the turbulent structures.

Conceptual Overview

- Schur decomposition $\mathcal{A} = \mathcal{U}\mathcal{T}\mathcal{U}^*$ which $\mathcal{T} = \mathbf{\Lambda} + \mathcal{N}$
  - $\mathbf{\Lambda}$ is diagonal matrix whose elements correspond to the eigenvalues of $\mathcal{A}$
  - $\mathcal{N}$ is an upper triangular matrix that represents the non-normal part of $\mathcal{A}$
- Tensors of the additive decomposition $\mathcal{A} = \mathcal{B}^{\mathcal{A}} + \mathcal{C}^{\mathcal{A}}$ are defined as

$$\mathcal{B}^{\mathcal{A}} = \mathcal{U}\mathbf{\Lambda}\mathcal{U}^*$$
$$\mathcal{C}^{\mathcal{A}} = \mathcal{U}\mathcal{N}\mathcal{U}^*$$

[‡] Keylock, C. J.
The Schur decomposition of the velocity gradient tensor for turbulent flows
Journal of Fluid Mechanics (2015).

- Characterize flow structures in the vicinity of evaporation fronts in a forced homogeneous isotropic turbulence.
- Two-component incompressible flows solver `Aphrós` [†].

$$\begin{cases} \nabla \cdot \mathfrak{u} = 0, \\ \partial_t \mathfrak{u} + \nabla \cdot (\mathfrak{u}\mathfrak{u}) = -\frac{1}{\rho}\left[\nabla \mathfrak{p} + \nabla \cdot (2\mu\mathcal{S}) + \underbrace{\boldsymbol{f}_\sigma}_{\sigma\kappa\boldsymbol{n}\delta(s)}\right] + \underbrace{\boldsymbol{f}}_{\frac{\epsilon - \mathcal{G}(\mathcal{K}-\mathcal{K}_\infty)\tau_\infty}{\langle \widetilde{\mathfrak{u}\cdot\mathfrak{u}} \rangle}\widetilde{\mathfrak{u}}} \end{cases} \quad (1)$$

- Turbulent kinetic energy of the velocity field is sustained at a desired level using a control-based linear forcing approach[‡‡].
- VOF/PLIC with piecewise linear reconstruction
- Marching cubes algorithm to compute the distance from the interface [††].

[†] Karnakov, P. and Wermelinger, F. and Litvinov, S. and Koumoutsakos, P.
`Aphrós`: *High Performance Software for Multiphase Flows with Large Scale Bubble and Drop Clusters*
Proceedings of the Platform for Advanced Scientific Computing Conference (2020).

[††] Lewiner, T. and Lopes, H. and Vieira, A. W. and Tavares, G.
Efficient implementation of marching cubes' cases with topological guarantees
Journal of Graphics Tools (2003).

[‡‡] Bassenne, M. and Urzay, J. and Park, G. I. and Moin, P.
EConstant-energetics physical-space forcing methods for improved convergence to homogeneous-isotropic turbulence with application to particle-laden flows
Physics of Fluids (2016).

➯ Computational setup

$\rho_\ell/\rho_\mathfrak{g}$	$\mu_\ell/\mu_\mathfrak{g}$	σ [N.m^{-1}]	L [m]	ϕ_ℓ	$\mathcal{W}\mathfrak{e}_\mathfrak{g}$
30	30	0.0135	1.5×10^{-4}	0.10	2.0
$\mathcal{W}\mathfrak{e}_\ell$	Re_ℓ	Re_λ	$\mathcal{O}\mathfrak{h}_\ell$	$\Delta x/\eta_\mathfrak{g}$	$\lambda/\eta_\mathfrak{g}$
60	620	31.25	0.0125	1.78	11.00

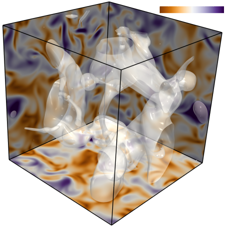

➯ Assessment of mesh convergence

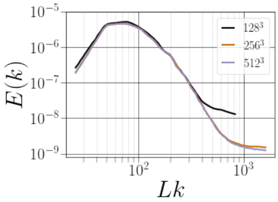

Small-scale effects are resolved on the resolution mesh featuring 512^3 grid points.

➯ Three layers are considered

- $-2.8 < \Phi/\eta_\mathfrak{g} < 0$ (near the droplets surface)
- $-7 < \Phi/\eta_\mathfrak{g} < -2.8$ (intermediate region between the carrier-fluid and the droplet)
- $\Phi/\eta_\mathfrak{g} < -7$ (far from the droplets).

INVARIANTS OF $\mathcal{A}$, $\mathcal{S}^{\mathcal{A}}$ AND $\Omega^{\mathcal{A}}$

➯ $(Q^{\mathcal{A}}, R^{\mathcal{A}})$ diagrams

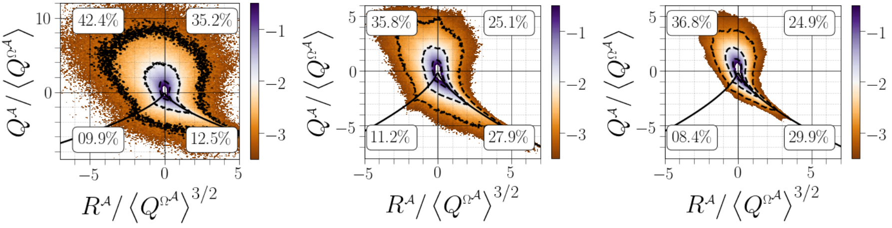

(a) Close (b) Intermediate (c) Far

➯ The joint PDF of the $(R^{\mathcal{A}}, Q^{\mathcal{A}})$ map exhibit a characteristic teardrop shape at Far.

➯ The isocontours tend to broaden and increase monotonically as the carrier–liquid interface is approached.

Invariants of $\mathcal{A}$, $\mathcal{S}^{\mathcal{A}}$ and $\Omega^{\mathcal{A}}$

- $(Q^{\mathcal{S}^{\mathcal{A}}}, R^{\mathcal{S}^{\mathcal{A}}})$ diagrams

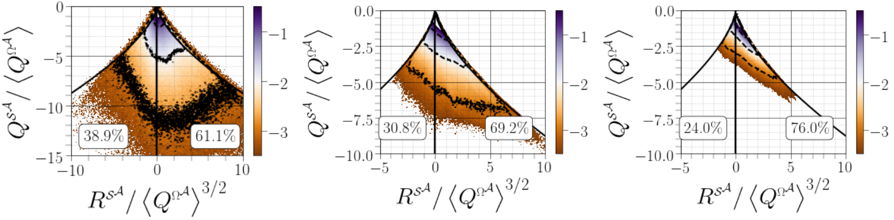

(a) Close (b) Intermediate (c) Far

- Decreasing preference for a rate-of-strain topology of the type saddle-saddle-unstable-node (two positive eigenvalues and one negative.
- The joint PDF of $(R^{\mathcal{S}^{\mathcal{A}}}, Q^{\mathcal{S}^{\mathcal{A}}})$ becomes slightly tilted towards $R^{\mathcal{S}^{\mathcal{A}}} > 0$ and tends to be symmetric along $R^{\mathcal{S}^{\mathcal{A}}} = 0$.

INVARIANTS OF $\mathcal{A}$, $\mathcal{S}^{\mathcal{A}}$ AND $\Omega^{\mathcal{A}}$

- $(Q^{\Omega^{\mathcal{A}}}, -Q^{\mathcal{S}^{\mathcal{A}}})$ diagrams

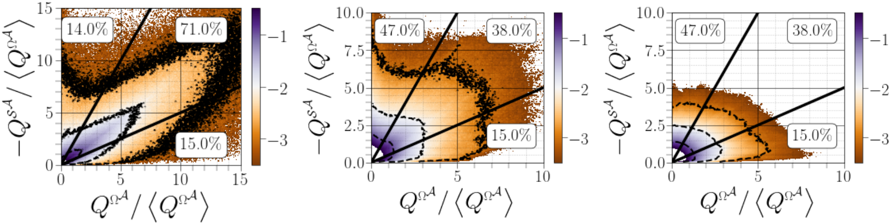

(a) Close (b) Intermediate (c) Far

- The joint PDF of $(Q^{\Omega^{\mathcal{A}}}, -Q^{\mathcal{S}^{\mathcal{A}}})$ shows a marked tendency to be aligned with the vertical line defined by $Q^{\Omega^{\mathcal{A}}} = 0$ in the closest region from the carrier–liquid interface.
  - Predominance of dissipation (strain production) over enstrophy

Estimate of the non-normality effects

Use of standardized difference to understand when the non-normal effects are significant

$$\kappa_{\mathcal{B},\mathcal{C}} = \frac{\|\mathcal{B}\| - \|\mathcal{C}\|}{\|\mathcal{B}\| + \|\mathcal{C}\|}.$$

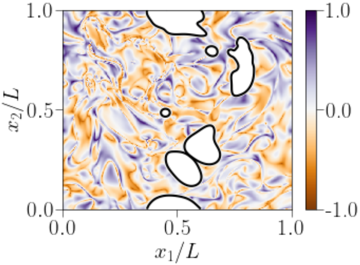

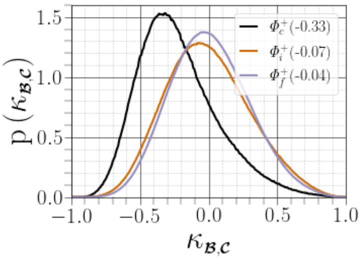

- The overall mode of the distribution of $\kappa_{\mathcal{B},\mathcal{C}}$ is slightly negative.
  - Non–normal effects in the dynamics of two–phase homogeneous isotropic turbulent flow are significant to $\mathcal{A}$ relative to the eigenvalues.
  - Similar tendencies have previously been noted for single phase HIT

Normal and non–normal effects on the dynamics of $\mathcal{A}$

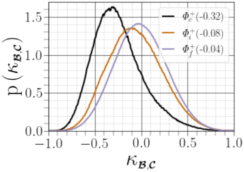

(a) UFC

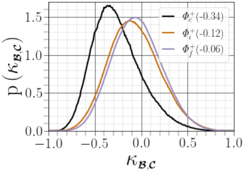

(b) SFS

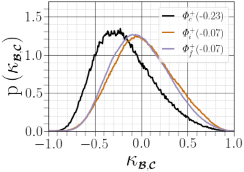

(c) SNSS

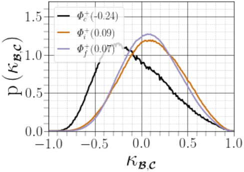

(d) UNSS

- The contribution of $\|\mathcal{C}\|$ becomes higher where $R^{\mathcal{A}} < 0$
- The departure from the zero mode is reduced far from the interface

Alignment of vorticity vector and strain–rate eigenvectors

- The alignment of $\boldsymbol{\omega}^{\mathcal{A}}$ with the principal strain rate axes directly influences the sign of $\omega_i^{\mathcal{A}}\omega_j^{\mathcal{A}}\mathcal{S}_{ij}^{\mathcal{A}}$.
  - $\omega_i^{\mathcal{A}}\omega_j^{\mathcal{A}}\mathcal{S}_{ij}^{\mathcal{A}} > 0$ indicate the production of enstrophy, whereas $\omega_i^{\mathcal{A}}\omega_j^{\mathcal{A}}\mathcal{S}_{ij}^{\mathcal{A}} < 0$ corresponds to the attenuation of enstrophy by vortex compression.

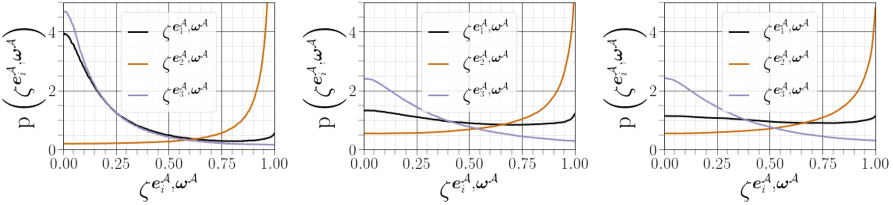

(a) Close (b) Intermediate (c) Far

- The obtained alignments agree with the findings of both single phase HIT.
- Close to the interface
  - The parallel alignment of $\boldsymbol{\omega}^{\mathcal{A}}$ with $\mathbf{e}_2^{\mathcal{A}}$ becomes more likely.
  - A higher frequency of orthogonality is observed between $\boldsymbol{\omega}^{\mathcal{A}}$ and $\mathbf{e}_3^{\mathcal{A}}$.
  - No special orientation of $\boldsymbol{\omega}^{\mathcal{A}}$ and $\mathbf{e}_1^{\mathcal{A}}$.

Alignment of vorticity vector and strain–rate eigenvectors

PDFs of the cosines of angles between the vorticity vector and strain eigenvectors for $\boldsymbol{\mathcal{A}}$, $\boldsymbol{\mathcal{B}}$ and $\boldsymbol{\mathcal{C}}$ (solid lines for Close, dashed lines for Intermediate, and dotted lines for Far).

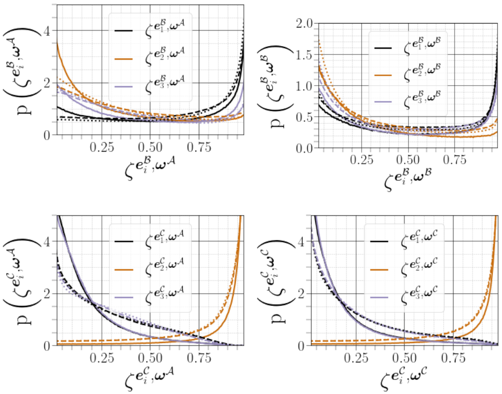

- A strong alignment between $\boldsymbol{\mathcal{A}}$ and $\lambda_2^{\mathcal{A}}$ when considering only the non–normal contribution of $\boldsymbol{\mathcal{A}}$, with a noticeable anti-alignment between $\lambda_1^{\mathcal{A}}$ and $\lambda_3^{\mathcal{A}}$
- The alignment between $\boldsymbol{\omega}^{\mathcal{A}}$ and $\lambda_2^{\mathcal{A}}$ is less strong in the vicinity of the liquid–gas interface

Conclusion

- This approach provides a means to link the eigenvalue and strain-rotation based approaches to studying the VGT.
- The results clarify the way in which the different topology in different parts of $Q^{\mathcal{A}} - R^{\mathcal{A}}$ space affect the kinematics and dynamics of the flow.
- The joint PDFs of velocity-gradient, rate-of-strain, and rate-of-rotation tensors far from the liquid–gas interface closely resemble canonical and universal single-phase homogeneous isotropic turbulence.
- Close to the interface with the liquid-pockets, the flow topology exhibits a boundary-layer-like flow with a predominance of vortex sheets.

Perspectives

- The next stage is to revisit some of the modeling approaches that already exist and to see if we can develop them in a more effective fashion using this approach.
- Moving beyond the HIT test case.
- Adapt SGS subgrid modelling to capture droplets interface

$$\tau_{ij}^{d} = -2\overline{\varrho}\Delta^2 \left(C_{\mathcal{B}} \left| \widetilde{\mathcal{S}^{\mathcal{B}}} \right| + C_{\mathcal{C}} \left| \widetilde{\mathcal{S}^{\mathcal{C}}} \right| \right) \left(\widetilde{\mathcal{S}_{ij}^{\mathcal{A}}} - \frac{1}{3}\delta_{ij} \widetilde{\mathcal{S}_{kk}^{\mathcal{A}}} \right), \quad (2)$$

Thanks for tuning in!
Please leave comments & questions

Acknowledgments

ASCC
AFRICAN
SUPERCOMPUTING
CENTER